The Effect of Electrode Structure on Ferroelectric Domains in Hf0.5Zr0.5O2

Tristan O'Neill, Yueyun Chen, Ho Leung Chan, Megan K Lenox, William A Hubbard, Jon F Ihlefeld, B C Regan

Microscopy and Microanalysis, **31** (7), 2025, 1084–1085
https://doi.org/10.1093/mam/ozaf048.567

Microscopy AND Microanalysis

Proceedings

The Effect of Electrode Structure on Ferroelectric Domains in $Hf_{0.5}Zr_{0.5}O_2$

Tristan O'Neill[1,2], Yueyun Chen[1,2], Ho Leung Chan[1,2], Megan K. Lenox[3], William A. Hubbard[4], Jon F. Ihlefeld[3,5], and B.C. Regan[1,2,*]

[1]*Department of Physics and Astronomy, University of California, Los Angeles, California, USA*
[2]*California NanoSystems Institute (CNSI), University of California, Los Angeles, California, USA*
[3]*Department of Material Science and Engineering, University of Virginia, Charlottesville, VA, USA*
[4]*NanoElectronic Imaging, Inc., Los Angeles, CA, USA*
[5]*Charles L. Brown Department of Electrical and Computer Engineering, University of Virginia, Charlottesville, VA, USA*

*Corresponding author: regan@physics.ucla.edu

Ferroelectric (FE) memory is poised to bridge the gaps in speed and bit density that exist between standard volatile and non-volatile memory technologies [1]. These "universal memory" technologies, if realized, will have profound impacts on modern computing. $Hf_{0.5}Zr_{0.5}O_2$ (HZO) is the leading material candidate for FE memory because it is CMOS compatible, it has a large spontaneous polarization, and its ferroelectricity has been demonstrated in films as thin as 3 nm [2]. But despite being one of the most studied materials of the last decade, its phase diagram remains poorly understood. In bulk, the FE orthorhombic phase of HZO (space group $Pca2_1$) is not stable. In thin films, it competes with several other non-FE phases of similar free energies; real devices typically contain a polymorphic and polycrystalline structure [1, 3-6]. An understanding of the microscopic details of real, operating devices would be extremely beneficial for the further development of HZO for FE memory applications.

Because it is only stable in thin films, encapsulating electrodes are widely believed to play a role in stabilizing the FE orthorhombic phase [3]. Indeed, the choice of electrode material has been shown to influence the HZO's ferroelectric properties dramatically [5]. Here, we study an HZO capacitor with TiN electrodes suspended on an electron-transparent Si_3N_4 membrane (**Fig. 1a**). As-deposited, the HZO film is amorphous, but it is crystallized *in situ* with a resistive heater. Annular dark field (ADF) scanning transmission electron microscopy (STEM) images reveal grain boundaries across the device in both the HZO and TiN layers, while simultaneously acquired STEM electron beam-induced current (EBIC) images show the existence of a spontaneous polarization across the device (**Fig. 1c-e**) [6-7]. No obvious correlation between the grain sizes or locations in the two media is evident from the ADF images. The HZO grains tend to be roughly an order of magnitude larger than those of the TiN, despite the materials' comparable thicknesses.

Because of the crystalline encapsulating electrodes and the structural similarity between the different phases present in the HZO layer, it is difficult to perform high resolution crystallographic phase mapping with techniques such as 4D STEM. Instead, we turn to the EBIC imaging modality. Surprisingly, STEM EBIC reveals that FE domain walls tend to coincide with the grain boundaries in the TiN electrodes – the structure of the encapsulating electrodes is imprinted onto the FE domain structure (**Fig. 2**). We conclude that the FE domain sizes are limited by the grain size of the TiN electrodes; they are much smaller than the HZO grains.

An understanding of how the FE orthorhombic phase of HZO is stabilized in thin films is crucial to the ultimate commercial development of HZO-based FE memory technologies. But distinguishing between the various structurally similar phases that HZO can take on in an operating device with high resolution remains a challenge. Our approach sheds light on how the encapsulation layers affect the stability of the FE phase in HZO. Further understanding of the crystallization pathways will allow for engineering the FE phase in these devices [10].

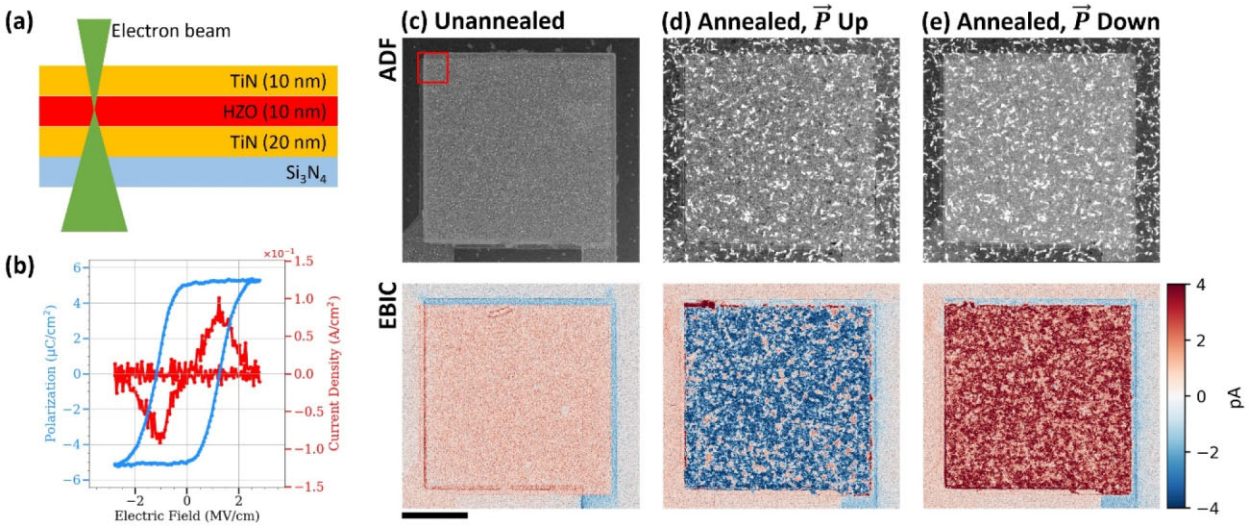

Fig. 1. Device Overview. (a) A cartoon illustrating the cross section of the devices under study (not to scale). The HZO is deposited *via* atomic layer deposition. It is amorphous as-deposited; annealing is necessary to crystallize it. The TiN electrodes are deposited via sputter coating. The structure is studied with STEM in plan-view. **(b)** A representative hysteresis loop from the device, obtained using a variation of the "positive-up, negative-down" (PUND) technique called nano-PUND [8-9], which shows that the device is ferroelectric. ADF (top) and EBIC (bottom) STEM images acquired prior to **(c)** and after **(d-e)** annealing. After annealing, the device is imaged in its two fully polarized states. HZO grain structure is clearly visible in the ADF images even where the HZO is sandwiched between the encapsulating TiN electrodes. The corresponding EBIC images show the electronic effect of the device's polarization state. The scale bar is 1 μm.

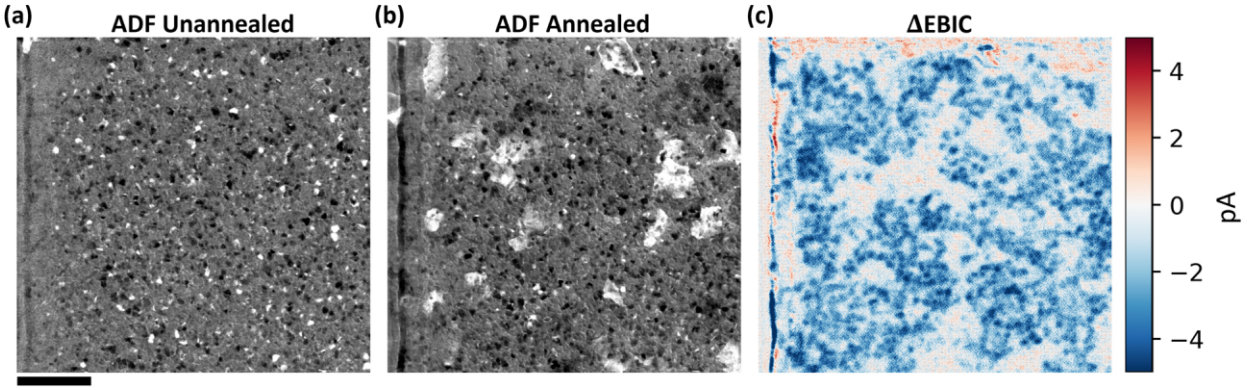

Fig. 2. Higher Magnification View of the Device. Higher magnification view of the region indicated in red in Fig. 1c. ADF STEM images obtained before **(a)** and after **(b)** annealing. The TiN grain sizes appear to be comparable to the overall thicknesses of the TiN layers (Fig. 1a). The HZO grains are only present after annealing, and are as much as an order of magnitude larger than the TiN grains. **(c)** Subtracting STEM EBIC images acquired in each polarization state reveals what regions of the device are ferroelectric. The scale bar is 100 nm.

References

1. Kim K *et al. Nature Nanotechnology* (2023) **18** 422-441. https://doi.org/10.1038/s41565-023-01361-y
2. Wang C *et al. Journal of Materials Chemistry C* (2021) **9** 12759-12767. https://doi.org/10.1039%2Fd1tc01778k
3. Materlik R *et al. Journal of Applied Physics* (2015) **117** 134109. https://doi.org/10.1063/1.4916707
4. Lederer M *et al. Applied Physics Letters* (2019) **115** 222902. https://doi.org/10.1063/1.5129318
5. Alcala R *et al. Advanced Functional Materials* (2023) **33** 2303261. https://doi.org/10.1002%2Fadfm.202303261
6. Chan HL *et al. ACS Nano* (2024) **18** 20380–20388. https://doi.org/10.1021/acsnano.4c04526
7. Hubbard W *et al. Physical Review Applied* (2018) **10** 044066. https://doi.org/10.1103/PhysRevApplied.10.044066
8. Scott JF. *Journal of Applied Physics* (1988) **64** 787–792. https://doi.org/10.1063/1.341925
9. Martin S *et al. Review of Scientific Instruments* (2017) **88** 023901. https://doi.org/10.1063/1.4974953
10. Data were acquired at the Electron Imaging Center for Nanomachines (EICN) at the University of California, Los Angeles's California for NanoSystems Institute (CNSI). This work is supported by the National Science Foundation (NSF) Science and Technology Center (STC) award DMR-1548924 (STROBE). This research is also supported by the Semiconductor Research Corporation (SRC) via tasks 2875.001 and 3293.001 within the Global Research Collaboration program.